Atomic oxygen adsorption and incipient oxidation of the Pb(111) surface: A density-functional theory study

Bo Sun, Ping Zhang,* Zhigang Wang, Suqing Duan, and Xian-Geng Zhao

Institute of Applied Physics and Computational Mathematics,

P.O. Box 8009, Beijing 100088, People's Republic of China

Xuchun Ma and Qi-Kun Xue

Institute of Physics, Chinese Academy of Sciences,

Beijing 100080, People's Republic of China

Abstract

We study the atomic oxygen adsorption on Pb(111) surface by using density-functional theory within the generalized gradient approximation and a supercell approach. The atomic and energetic properties of purely on-surface and subsurface oxygen structures at the Pb(111) surface are systematically investigated for a wide range of coverages and adsorption sites. The fcc and tetra-II sites (see the text for definition) are found to be energetically preferred for the on-surface and subsurface adsorption, respectively, in the whole range of coverage considered. The on-surface and subsurface oxygen binding energies monotonically increase with the coverage, and the latter is always higher than the former, thus indicating the tendency to the formation of oxygen islands (clusters) and the higher stability of subsurface adsorption. The on-surface and subsurface diffusion-path energetics of atomic oxygen, and the activation barriers for the O penetration from the on-surface to the subsurface sites are presented at low and high coverages. In particular, it is shown that the penetration barrier from the on-surface hcp to the subsurface tetra-I site is as small as 65 meV at low coverage (Θ=0.25). The other properties of the O/Pb(111) system, including the charge distribution, the lattice relaxation, the work function, and the electronic density of states, are also studied and discussed in detail, which consistently show the gradually stabilizing ionic O-Pb bond with increase of the oxygen coverage.

*Corresponding author. Electronic address: zhang_ping@iapcm.ac.cn

I. INTRODUCTION

Lead (Pb) is one kind of heavy metal element with widespread availability. Single crystal Pb is extremely resistant to oxygen [1]. Appreciable oxidation takes place only at relatively high temperature ($\geqslant$370K) or at considerable oxygen coverage at room temperature. However, this inoxidability of lead can be overcome by a so-called two-step treatment [2]: (i) low temperature (100K) adsorption, followed by (ii) annealing at elevated temperatures to above 220K. The method itself proves to be a very effective way for low-temperature surface oxidation. Using this two-step approach, recently, the oxygen adsorption on ultra-thin Pb(111) films was experimentally investigated by using the scanning tunneling microscopy (STM) and scanning tunneling spectroscopy (STS) measurements [3]. Remarkably, it was found that the surface oxidation displays a prominent quantum oscillating effect by varying the thickness of Pb(111) film. Furthermore, it was found that the O adsorbates can form some magic clusters with regular size and shape [4]. These phenomena of the oxygen adsorption and surface oxidation at Pb(111) remain yet to be exploited and understood, which is a main driving force for our present first-principles study. Contrary to the extensive first-principles studies of the surface oxidation on transition metals (TMs) such as Cu [5–13], Ag [14–25], Rh [26–30], Pd [31–35], Pt [36–40], and Ru [41, 42], and on the simple *sp* metals such as Al [43–49] and Mg [50–52], *ab initio* studies of oxygen chemisorption on Pb(111) surface, in particular, O subsurface species on Pb(111) surface, are still lacking.

In this paper, we have carried out the first-principles calculations of the on-surface and the subsurface O adsorption at Pb(111) in a wide range of coverages. Results for the determination of stable adsorption sites, work-function and atomic-relaxation changes, charge densities, electronic structures, and energy barriers for O diffusion and penetration, are systematically presented. Like the other metals, the surface oxidation of Pb is expected to involve three main events: (i) the initial dissociation of O_2 molecules and the oxygen chemisorption on Pb(111) surface, followed by (ii) lattice penetration of atomic oxygen and oxide nucleation, and finally (iii) the crystallization and growth of the stoichiometric oxide phases. The sequence of these events may be complex, and rather than successively, they may occur simultaneously, depending on the temperature and pressure. The main purpose of this paper is to give a partial but detailed understanding of events (i) and (ii) by studying the energetics and structures of atomic O adsorbates with purely on-surface and subsurface

adsorption sites and with different coverages. A full study involving the initial dissociation of O_2 molecules when approaching to or accumulating on the Pb(111) surface, and the penetration process which involves simultaneous on-surface and sub-surface adsorption, will be given elsewhere. In particular, since the atomic oxygen adsorption and diffusion on metal surface are elementary processes towards the whole surface oxidation, and the atomic configuration after the oxygen chemisorption may give a reasonable foresee for the tendency of bulk oxidation, it is expected that the present systematic first-principles calculations of the oxygen adsorption on Pb(111) is of highly interest in relation to understanding the nature of the O-Pb bond in general and of great necessity.

This paper is organized as follows. In Sec. II we give details of the first-principles total energy calculations, which is followed in Sec. III by our results for bulk Pb, the clean Pb(111) surface, and the O_2 molecule. The results for purely on-surface adsorption as a function of the oxygen coverage are presented in Sec. IV, where the surface and adsorption energetics, the atomic geometry, and the electronic structures are presented and analyzed. In Sec. V, we discuss the purely subsurface adsorption of oxygen atoms as we did in Sec. IV. The energy barriers for atomic oxygen diffusion and penetration are presented in Sec. VI, and the conclusion is given in Sec. VII.

II. THE CALCULATION METHOD

The density-functional theory (DFT) total energy calculations were carried out using the Vienna *ab initio* simulation package [53] with the projector-augmented-wave (PAW) pseudopotentials [54] and plane waves [55]. In the present film calculations, the so-called *repeated slab* geometries were employed [56]. This scheme consists in the construction of a unit cell of an arbitrarily fixed number of atomic layers identical to that of the bulk in the plane of the surface (defining the bi-dimensional cell), but symmetrically terminated by an arbitrarily fixed number of empty layers (the "*vacuum*") along the direction perpendicular to the surface. In the present study, the clean Pb(111) surface is modeled by periodic slabs consisting of ten lead layers separated by a vacuum of 20 Å, which is found to be sufficiently convergent. The oxygen atoms are adsorbed on both sides of the slab in a symmetric way. During our calculations, the positions of the outmost three lead layers as well as the O atoms are allowed to relax while the central four layers of the slab are fixed in their calculated bulk

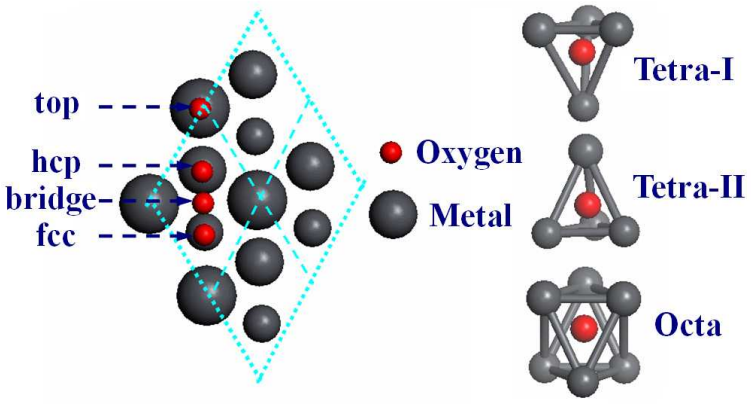

FIG. 1: (Color online) (Left panel) four on-surface adsorption sites including fcc, hcp, bridge (B2), and on-top (T1) sites. Note that Pb atoms of outmost three layers are shown by scaled grey balls (the largers are outer Pb atoms). (Right panel) three subsurface adsorption sites including tetra-I, tetra-II, and octa sites.

positions. The plane-wave energy cutoff was set 400 eV. If not mentioned differently we have used a $(12 \times 12 \times 1)$ k-point grid for the p(1×1) surface cell, $(6 \times 6 \times 1)$ k-point grid for the p$(\sqrt{3} \times \sqrt{3})$ and p(2×2) cells, and $(4 \times 4 \times 1)$ k-point grid for the p(3×3) cell, with Monkhorse-Pack scheme [60]. The use of larger k-point meshes did not alter these values significantly. Furthermore, the generalized gradient approximation (GGA) of Perdew *et al.* [58] for the exchange-correlation potential was employed. A Fermi broadening [59] of 0.05 eV was chosen to smear the occupation of the bands around E_F by a finite-T Fermi function and extrapolating to $T = 0$ K.

In the present paper, the calculations for oxygen atoms in the five adsorption sites, including on-surface (hcp and fcc) and subsurface (tetra-I, tetra-II, and octa) sites depicted in Fig. 1, have been performed for coverage ranging from 0.11 ML to a full monolayer. Specially, the oxygen coverages of 0.11 ML, 0.33 ML, and 0.67 ML were calculated using p(3×3) surface unit cell, while the coverages of 0.25 ML, 0.50 ML, 0.75 ML, and 1.0 ML were calculated in the p(2×2) surface cell containing one, two, three, and four oxygen atoms, respectively. The on-surface top (T1) and the bridge (B2) adsorption sites were also considered. The T1 site was found to be notably less favorable than the fcc and hcp sites. When the O atom is placed on the B2 site, it always moves to the fcc site after relaxation. Actually, figure 15 below will show that the B2 site is a saddle point in the O diffusion

path from hcp to fcc site. Thus in this paper, most of the on-surface adsorption studies are focused on the fcc and hcp sites.

One central quantity tailored for the present study is the average binding energy of the adsorbed oxygen atom defined as

$$E_b(\Theta) = -\frac{1}{N_{\rm O}}[E_{\rm O/Pb(111)} - E_{\rm Pb(111)} - N_{\rm O}E_{\rm O}], \tag{2}$$

where $N_{\rm O}$ is the total number of O atoms (on-surface and subsurface) present in the supercell at the considered coverage Θ (we define Θ as the ratio of the number of adsorbed atoms to the number of atoms in an ideal substrate layer). $E_{\rm O/Pb(111)}$, $E_{\rm Pb(111)}$, and $E_{\rm O}$ are the total energies of the slab containing oxygen, of the corresponding clean Pb(111) slab, and of a free O atom respectively. According to this definition, E_b is also the adsorption energy $E_{\rm ad}$ per O atom, i.e., the energy that a free O atom gains upon its adsorption. Thus a positive value of E_b indicates that the adsorption is exothermic (stable) with respect to a free O atom and a negative value indicates endothermic (unstable) reaction. On the other hand, since in most cases, the oxygen chemisorption process inevitably involves the dissociation of O_2 molecules, thus the adsorption energy per oxygen atom can alternatively be referenced to the energy which the O atom has in the O_2 molecule by subtracting half the dissociation energy D of the O_2 molecule,

$$E_{\rm ad(1/2O_2)} = E_b - D/2. \tag{3}$$

With this choice of adsorption energy, then a positive value indicates that the dissociative adsorption of O_2 is an exothermic process, while a negative value indicates that it is endothermic and that it is energetically more favorable for oxygen to be in the gas phase as O_2.

III. THE BULK PB, CLEAN PB(111) SURFACE, AND OXYGEN MOLECULE

First the total energy of the bulk fcc Pb was calculated to obtain the bulk lattice constant. The calculated lattice constant is a=5.028 Å, comparable well with experimental values of 4.95 Å[61]. The $6s$ and $6p$ electrons of the Pb atom were treated as the valence electrons and the $5d$ electrons were treated as core electrons. This choice of valence and core electrons has been previously employed to study the electronic properties of lead oxide (including PbO [62]

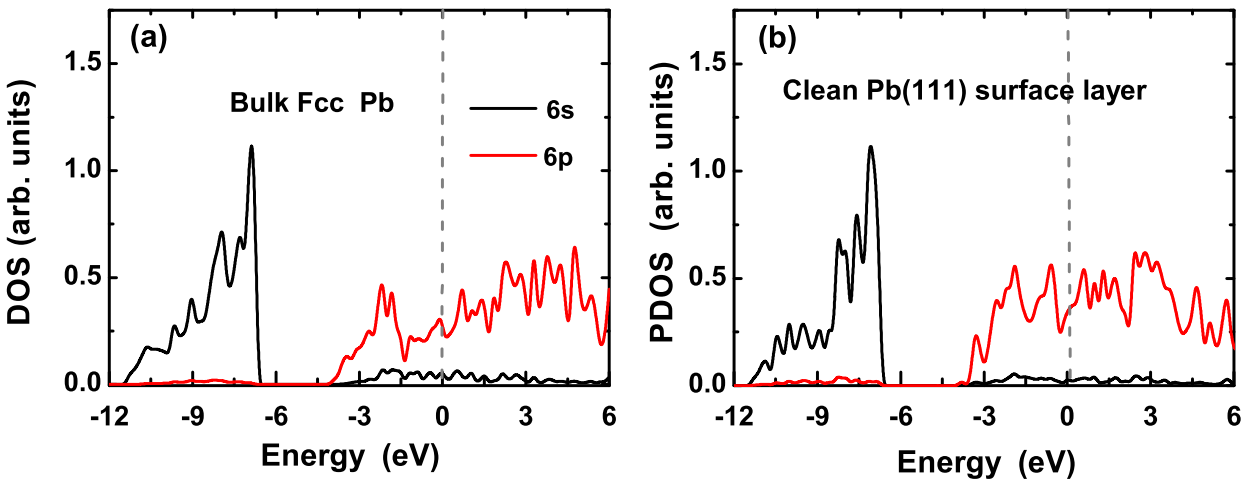

FIG. 2: (Color online) (a) Orbital-resolved DOS (per atom) for bulk Pb. (b) Orbital-resolved partial DOS for the clean 1×1 Pb(111) surface layer. The Fermi energy is indicated by the vertical dashed line at 0 eV.

and PbO_2 [63]). Note that we have also studied the effect of Pb 5d electrons on the surface properties of clean and oxygen-adsorbed Pb(111) surface and found no accountable changes by treating the Pb 5d electrons as valence electrons [64]. The orbital-resolved electronic density of states (DOS) per atom for the bulk Pb is shown in Fig. 2(a). The two broad peaks correspond to Pb $6s$ and $6p$ states. Compared to the $6s$ band, the $6p$ bands are more dispersive due to the extensive character of the atomic p orbitals. In addition, there is a small s-p hybridization near the Fermi energy.

The calculation for the atomic relaxations of the clean surface p(1×1), p$(\sqrt{3} \times \sqrt{3})$, p$(2 \times 2)$, and p$(3 \times 3)$ periodicities (models), provides not only a test of the clean surface with different cell sizes, but is also used to evaluate the charge density difference used later and assess the changes in the work function by the O adsorption. Our clean-surface calculations show that the two outmost Pb(111) layers relax significantly from the bulk values, namely, the first-second layer contraction is nearly 5% and the second-third layer expansion is nearly 3%, in agreement with the recent results from first-principles calculations [65] and the LEED experiment [66]. Note that the first interlayer separation on most metal surfaces is contracted, Pb(111) is also a typical example. The third-forth layer distance is practically the same as the interlayer distance in the bulk. The variation of the work function is negligible for different surface cells [with a value of 3.83 eV, see the inset in Fig. 7(a)

below] and is in excellent agreement with the other theoretical result [65]. The charge density $n(\mathbf{r})$ (not depicted here) shows that like the other typical surface calculations [67], there is a rapid variation in $n(\mathbf{r})$ in the surface interstitial region, with $n(\mathbf{r})$ falling off sharply in magnitude towards the vacuum and soon "healing" the discrete atomic nature of the surface. This sizable charge redistribution near the surface is associated with the formation of the (uniform) surface dipole layer, which sensitively determines the work function.

As one knows, surface calculations are very subtle, requiring enough k-point mesh and efficient energy cutoff, the correct model, and the other details. To test the convergency of the physical properties of the clean Pb(111) surface, we have calculated and analyzed the interlayer relaxations $\Delta_{ij}=(d_{ij}-d_0)/d_0$ with respect to the bulk interlayer distance d_0=2.903 Å, the surface energy E_s, and the work function Φ of the clean Pb(111) films by using different models with various k-points mesh. The results for different models are listed in Table I, from which it reveals that while the atomic interlayer relaxations are somewhat sensitive to the choice of k-points mesh and the model, the influences to the surface energetics from using different models are negligibly small. We suggest to analyze the surface energetics and electronic structures under the calculations of the same model, since the required high accuracy is expected to obtain by using the same surface model to do more reliable calculations and comparisons. For example, a p(3×3) surface unit cell is needed if one wants to analyze the properties of surface chemical activity in a coverage range beginning from Θ=0.11.

TABLE I: The calculated interlayer relaxation Δ_{ij} (%), surface energy E_s (in eV), and work function Φ (in eV) for different clean Pb(111) surface models with different k-point meshes.

Model	k-point mesh	irreducible k	Δ_{12} (%)	Δ_{23} (%)	Δ_{34} (%)	E_s (eV)	Φ (eV)
1×1	$12\times 12\times 1$	216	-4.670	2.560	-0.149	0.372	3.830
1×1	$6\times 6\times 1$	54	-5.326	3.066	-0.267	0.350	3.786
$\sqrt{3}\times\sqrt{3}$	$6\times 6\times 1$	54	-5.110	2.090	0.160	0.360	3.833
2×2	$6\times 6\times 1$	54	-4.803	2.977	-0.100	0.372	3.830
3×3	$4\times 4\times 1$	24	-4.882	2.890	0.369	0.373	3.832
3×3	$3\times 3\times 1$	5	-5.978	2.831	1.320	0.372	3.834

Figure 2(b) plots the orbital-resolved layer-projected density of states (PDOS) for the

topmost Pb layer of the clean p(1×1) Pb(111) surface cell. Compared to the Fig. 2(a), one can see that the surface electronic structure is almost the same as that of the bulk, with a little anisotropy in the p_x/p_y and p_z orbitals for the surface Pb atom. Note that throughout this paper we did not consider the quantum size effect on the atomic and electronic structures, since in our various supercell models the substrate has been fixed with the same thickness.

The total energies of the isolated O atom and the free O_2 molecule are calculated in a cubic cell of side length 10 Åwith a $(3 \times 3 \times 3)$ k-point mesh for the Brillouin zone sampling. The spin-polarization corrections to the O atom and the O_2 molecule are included. The binding energy of O_2 is calculated to be $1/2E_b^{O_2}$=3.12 eV per atom and the O-O bond length is about 1.235 Å. These results are typical for well-converged DFT-GGA calculations. Compared to the experimental [68] values of 2.56 eV and 1.21 Åfor O binding energy and bonding length, the usual DFT-GGA result always introduces an overestimation, which reflects the theoretical deficiency for describing the local orbitals of the oxygen. The resultant error in calculating the absolute value of the binding energy, however, does not matter in this work, since it is the difference in binding energies of two geometries that determines which one is more sable (if they contain the same amount of oxygen) or how E_b evolves with coverage (if the structures contain an unequal amount of O atoms). We will consider this overbinding of O_2 when drawing any conclusion that may be affected by its explicit value.

IV. THE PURE ON-SURFACE ADSORPTION

For different oxygen coverages Θ, the binding energies E_b for oxygen on the Pb(111) surface in the fcc and hcp sites, with respect to atomic oxygen, are illustrated in Fig. 3 and summarized in Table II. One can see from Fig. 3 that the binding energy for the O_{fcc} or O_{hcp} atom displays a modestly increasing tendency with the oxygen coverage, while the overall variation in the magnitude of E_b is rather small in the range of coverage we considered. The increasing binding energy with coverage indicates a prominent attraction between the on-surface oxygen atoms, implying a tendency to form the oxygen islands or clusters on the Pb(111) surface. This result is similar to that of the O-adsorbed Al(111) and Mg(0001) surfaces, compared to which the increasing slope in E_b-Θ curve in the present O/Pb(111) system is somewhat slower, but is in contrast to the oxygen/TMs due to the increasing

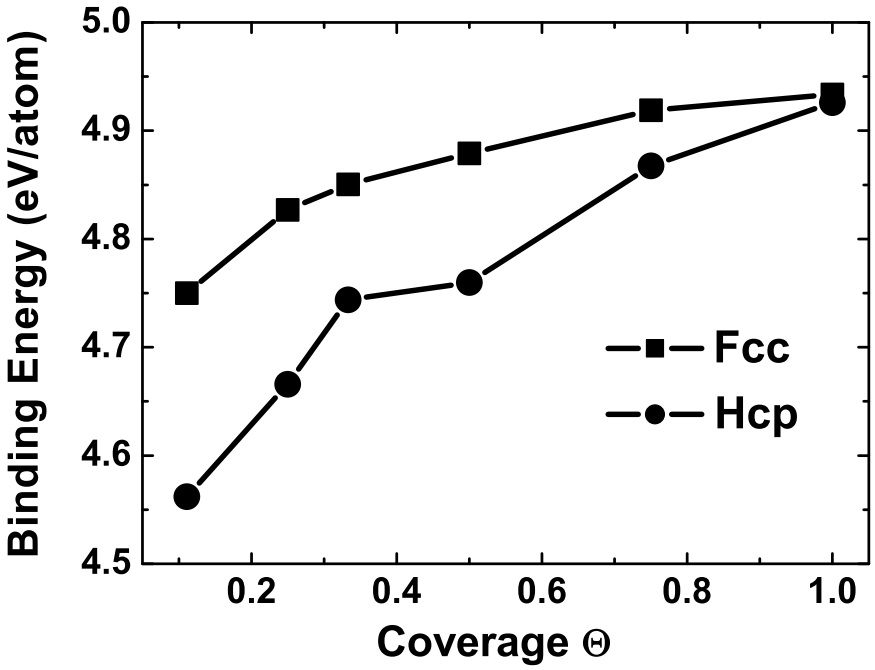

FIG. 3: Calculated binding energies of O/Pb(111) systems, with oxygen in the fcc (solid squares) and hcp (solid circles) sites, as functions of the oxygen coverage. The solid lines connecting the calculated binding energies are used to guide the eyes.

electron occupation of the antibonding states with the O coverage in those systems. On the other side, considering the binding energy E_b of atomic oxygen on the surface with respect to half the binding energy of the O_2 molecule (the calculated value of 3.12 eV or experimental value of 2.56 eV), we can see that the calculations predict that in the whole coverage range we considered, the atomic oxygen on-surface adsorption is stable. Also it reveals in Fig. 3 that the fcc site is energetically favorable relative to the hcp site, although their difference in E_b decreases with increasing Θ, namely, from 0.19 eV at Θ=0.11 down to (less than) 0.01 eV at Θ=1.0.

Table III presents the results for the relaxed atomic structures, including the height $h_{\text{O-Pb}}$ of O above the surface, the O-Pb bond length R_1, and the interlayer relaxations Δ_{ij} for various coverages with O in the fcc and hcp sites. For more clear illustration, the first and second interlayer relaxations (Δ_{12} and Δ_{23}), and the O-Pb bond length are also plotted in Fig. 4 and Fig. 5, respectively. One can see from Fig. 4 that the adsorption of oxygen on Pb(111) induces notable changes in the interlayer distances of the substrate

TABLE II: The calculated binding energy E_b (in eV) and work function Φ (in eV) as functions of oxygen coverage for five on-surface and subsurface adsorption sites.

	Site	Θ=0.11,	0.25,	0.33,	0.5,	0.75,	1.0
	fcc	4.750	4.827	4.850	4.879	4.919	4.934
	hcp	4.562	4.666	4.744	4.760	4.868	4.926
E_b	tetra-I	4.771	4.785	4.863	4.887	5.019	5.139
	tetra-II	4.842	4.907	4.927	4.957	5.053	5.145
	octa	4.628	4.545	4.776	4.876	4.862	5.012
	fcc	3.941	4.222	4.407	4.715	5.269	5.969
	hcp	3.966	4.253	4.485	4.749	5.236	5.994
Φ	tetra-I	3.812	3.759	3.736	3.499	3.490	3.148
	tetra-II	3.809	3.706	3.621	3.543	3.289	2.997
	octa	3.807	3.749	3.616	3.567	3.322	3.062

TABLE III: The calculated atomic interlayer relaxation Δ_{ij} (%), O-Pb bond length R_1 (in Å), and the adsorbate height $h_{\text{O-Pb}}$ (in Å) for different oxygen coverages of on-surface adsorption.

Coverage	$h_{\text{O-Pb}}$ (Å)		R_1 (Å)		Δ_{12} (%)		Δ_{23} (%)	
	fcc	hcp	fcc	hcp	fcc	hcp	fcc	hcp
0.11	1.116	1.115	2.282	2.289	-3.098	-3.567	1.752	-0.492
0.25	0.914	0.876	2.266	2.268	-1.641	-0.413	1.378	-0.601
0.33	1.047	0.939	2.257	2.274	-1.568	-0.095	0.779	-0.176
0.50	0.975	1.010	2.265	2.269	3.405	4.562	-0.614	-2.498
0.75	0.980	0.944	2.258	2.252	12.995	12.298	-2.445	-3.243
1.00	0.971	0.970	2.271	2.272	20.363	21.002	-5.085	-4.863

for the whole coverages considered. In particular, the topmost interlayer relaxation (Δ_{12}) changes from contraction (about -5%) to expansion (about 20%), and on the contrary, the second interlayer relaxation (Δ_{23}) changes from expansion (about 3%) to contraction (about -5%), for O in both fcc and hcp sites. This large and sign-inverted change of atomic interlayer relaxation by oxygen adsorption is unique for O/Pb(111) when comparing with the other oxygen/metal systems. For instance, at Al(111) surface, the topmost interlayer

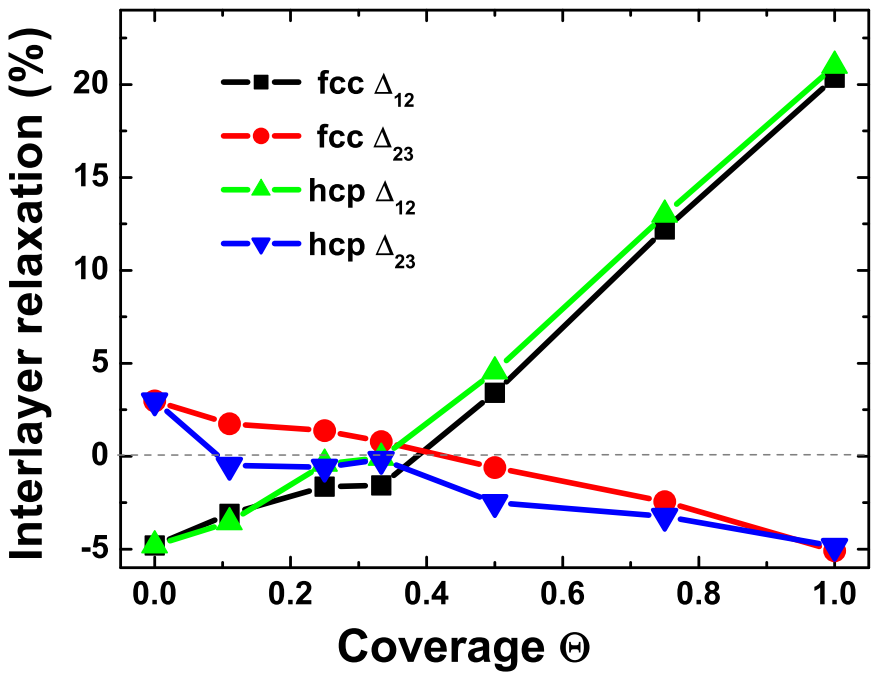

FIG. 4: (Color online) Atomic interlayer relaxations as functions of coverage for oxygen in fcc (solid square) and hcp (solid circle) sites.

relaxation on oxygen adsorption is at most Δ_{12}=4% [48], while at Ag(111) surface, there is even no change of interlayer relaxation before and after oxygen adsorption. The large expansion in Pb(111) interlayer relaxations reflects the strong influence of the O adsorbate on the neighboring Pb atoms, and will result in important redistribution of the electronic structure.

The O-Pb bond length R_1 for the fcc and hcp on-surface adsorption sites is shown in Fig. 5 as a function of the oxygen coverage Θ. One can see that for both fcc and hcp adsorption, the O-Pb bond length varies around 2.26 Åvery little with increasing Θ. In particular, the calculated results of R_1 by using the same $p(2 \times 2)$ surface model varies only within an amplitude of 0.01 Å(0.02 Å) for fcc (hcp) site. The short bond length R_1 implies a strong interaction between O and Pb atoms. Note that the value of R_1 in the fcc adsorption site is a little shorter than in the hcp site, which is consistent with the fact that the fcc site is more stable than the hcp site for on-surface adsorption.

Upon on-surface oxygen adsorption, the Pb atoms on the three outmost layers exhibit lateral and vertical displacements, which are plotted in Fig. 6 for energetically stable fcc

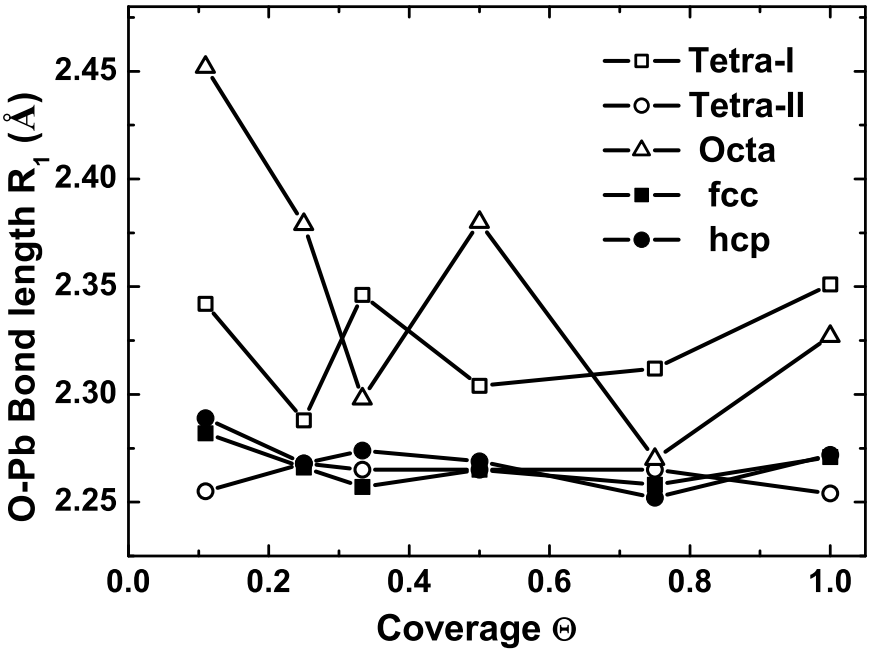

FIG. 5: The O-Pb bond length as a function of coverage for different on-surfce and subsurface adsorption sites.

adsorption at different coverages. From the left panel (atomic top view) of Fig. 6, one can see that Pb atoms bonded to oxygen in top layer always move outwards from chemisorbed oxygen for different coverages with the same p(2×2) surface model. The values of atomic movements are also indicated in the figure. The right panel (side view) of Fig. 6 depicts the vertical movements of Pb atoms from the center of mass of each layer. One prominent feature is that the oxygen at various coverages (except for the case Θ=1.0) we considered causes a most noticeable rumpling of the second Pb layer, which can be seen by large value of vertical movement of the second Pb layer.

We turn now to analyze the electronic properties of the O/Pb(111) system by first considering the work function Φ at different coverages and its change $\Delta\Phi$ with respect to the clean Pb(111) surface, both of which were illustrated in Fig. 7 and summaized in Table II. From Fig. 7(a), it can be seen that the work function slightly but steadily increases with O coverage for both fcc and hcp on-surface adsorption sites. Comparing with the other TM surfaces such as Ag(111), we notice that the varying amplitude of Φ in the whole coverages at the present Pb(111) surface is much smaller. In fact, from Fig. 7(b) one can see that the value of $\Delta\Phi$ varies from about 0.4 eV (at Θ=0.25) to about 2.1 eV (at Θ=1.0) for both fcc

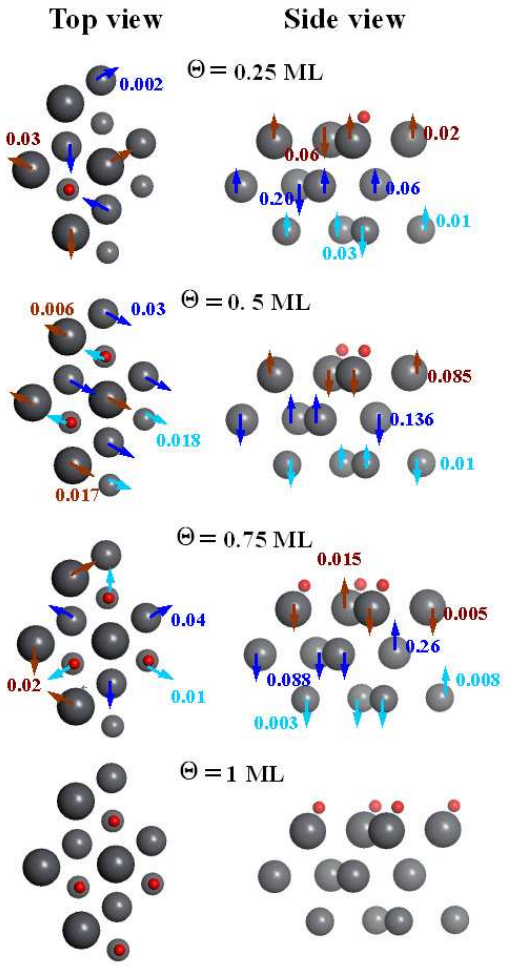

FIG. 6: (Color online) Different structures of oxygen adsorbed in the fcc site on Pb(111) surface. The left part shows the top view of the three outmost Pb layers. The right-hand part shows a side view of the vertical positions of the ions, cut in the plane along the $[1\bar{2}1]$ direction. Note, the gray balls with different scales, represent Pb atoms on the different layers (the lager is the outer), and the small red balls represent the oxygen atoms. The arrows (not to scale) indicate the directions of the atomic displacements, with different colors standing for different layers. The numbers that refer to the arrows are given in angstrom.

and hcp on-surface adsorption. Whereas, for O/Ag(111) system, $\Delta\Phi$ changes from about 1.2 eV at Θ=0.25 to 4.0 eV at at Θ=1.0 [20]. On the other side, our results of $\Delta\Phi$ versus Θ can be comparable with those for the other O-adsorbed *sp* simple metal surfaces such as Al(111) [48] and Mg(0001) [52]. Also from Fig. 7 it can be seen that the amplitude of $\Delta\Phi$ for the hcp adsorption site is a little more prominent than that of the fcc site.

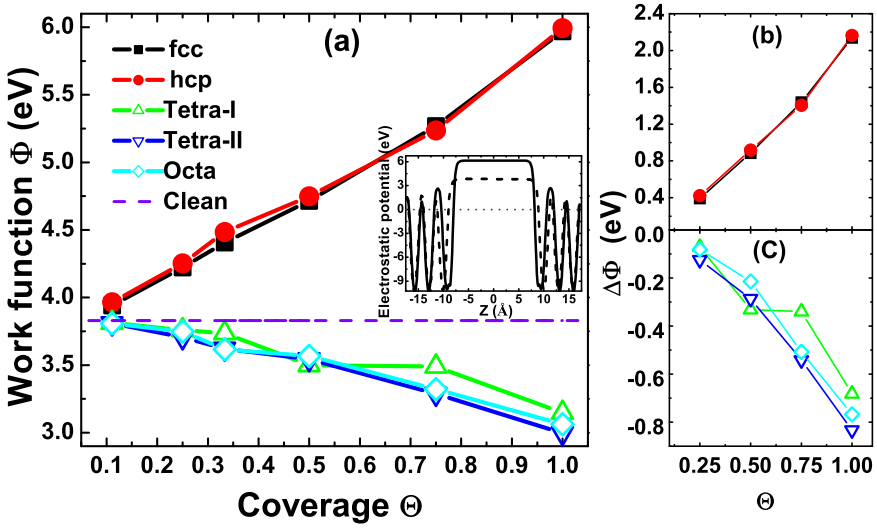

FIG. 7: (Color online) (a) The calculated work function Φ as a function of Θ for different on-surface and subsurface adsorption sites. The dashed line shows the value of Φ for clean Pb(111) substrate. (b) The change $\Delta\Phi$ in the work function by fcc and hcp on-surface O adsorption versus the coverage. (c) The quantity $\Delta\Phi$ for tetra-I, tetra-II, and octa subsurface adsorption sites. As an example, the inset in figure (a) shows the planar-averaged electrostatic potential of clean (dashed curve) and O-adsorbed (solid curve with Θ=1.0) Pb(111) slab, with the Fermi energies for both cases set to be zero.

To gain more insight into the nature of oxygen chemisorption on Pb(111) surface, we now analyze our results by means of the charge density difference $\Delta n(\mathbf{r})$ before and after O adsorption, and the orbital-resolved PDOS. Here the density difference $\Delta n(\mathbf{r})$ was obtained by subtracting the electron densities of noninteracting component systems, $n^{\mathrm{Pb(111)}}(\mathbf{r}) + n^{\mathrm{O}}(\mathbf{r})$, from the density $n(\mathbf{r})$ of the O/Pb(111) system, while retaining the atomic positions of the component systems at the same location as in O/Pb(111). Figures 8(a)-(b) (right panel in each figure) present the contour plots of $\Delta n(\mathbf{r})$ for Θ=0.25 and Θ=1.0, respectively. The total charge densities are also shown in the left panels. Such contour plots can provide physical insight into the nature of the chemical bonding. It reveals that the charge redistribution mainly occurs at the surface and involves the O adatom and the topmost Pb atoms. It is apparent that upon adsorption electrons flow into the O-2p orbitals. The influence of the adsorbed surface is rapidly screened out on going into the bulk. In fact, one can see that the bonding character of the inner Pb layers (from the second layer for Θ=0.25 and from the

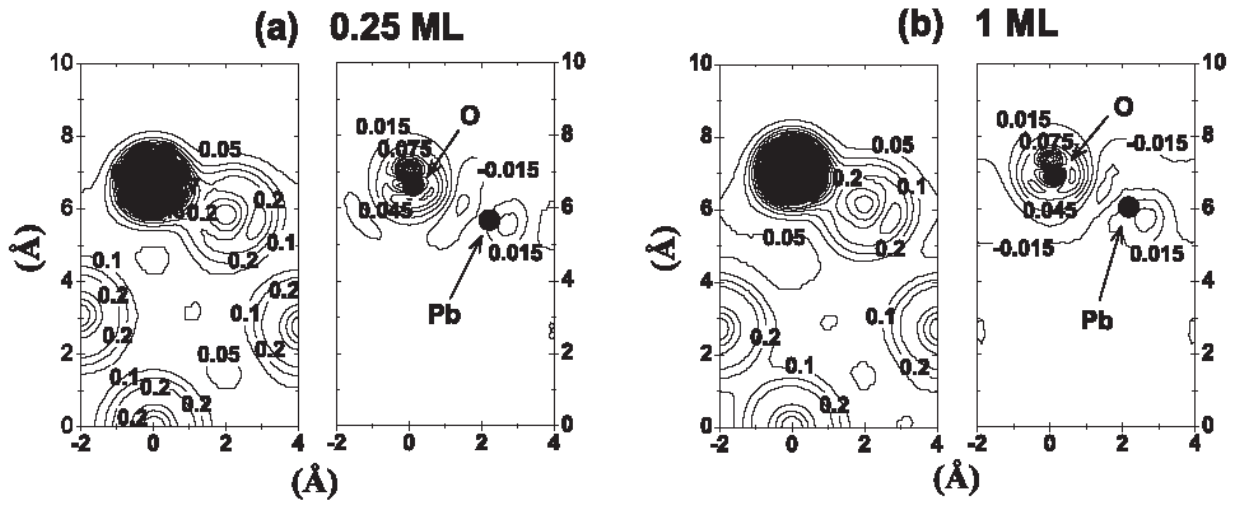

FIG. 8: Contour plots of the total valence charge density $n(\mathbf{r})$ (left panel) and the charge density difference $\Delta n(\mathbf{r})$ (right panel) for the on-surface O/Pb(111) slabs with the coverage (a) $\Theta = 0.25$ and (b) $\Theta = 1.0$. The contour plane is parallel with the $[1\bar{2}1]$ direction and is perpendicular to the Pb(111) surface.

third layer for Θ=1.0) is essentially identical to the bulk case, which is typically metallic with a fairly constant charge density between the atoms with slight directional bonding along the body diagonals. This is also emphasized by the density difference contour plots in Fig. 8 which reveals only very small changes in the interior of the nine-layer Pb slab. At both low (Θ=0.25) and high (Θ=1.0) coverages, one can see from Fig. 8 that the second-layer Pb atom and especially the surface Pb atom show remarkable changes in the charge density, reflecting the strong influence of the neighboring on-surface O atoms. It is also apparent in Fig. 8 that the bonding between O and surface Pb atoms is largely ionic in nature, which is is evident from the charge accumulation spherically centered on the O atom with radius $\sim$1.35 Åof ionic radius of O^{-2}) and the charge depletion between O and surface Pb atoms. The charge accumulation on the surface and charge depletion below the surface will result in the formation of a dipole moment (in line with the usual surface dipole layer) which tends to increase the work function as compared to that for the clean Pb(111) surface, as discussed above. Obviously, the charge transforms solely onto the O-2p orbitals. The shape of the density difference contour is similar for low and high coverages, indicating that the O-Pb bonding nature is keeps invariant when increasing the

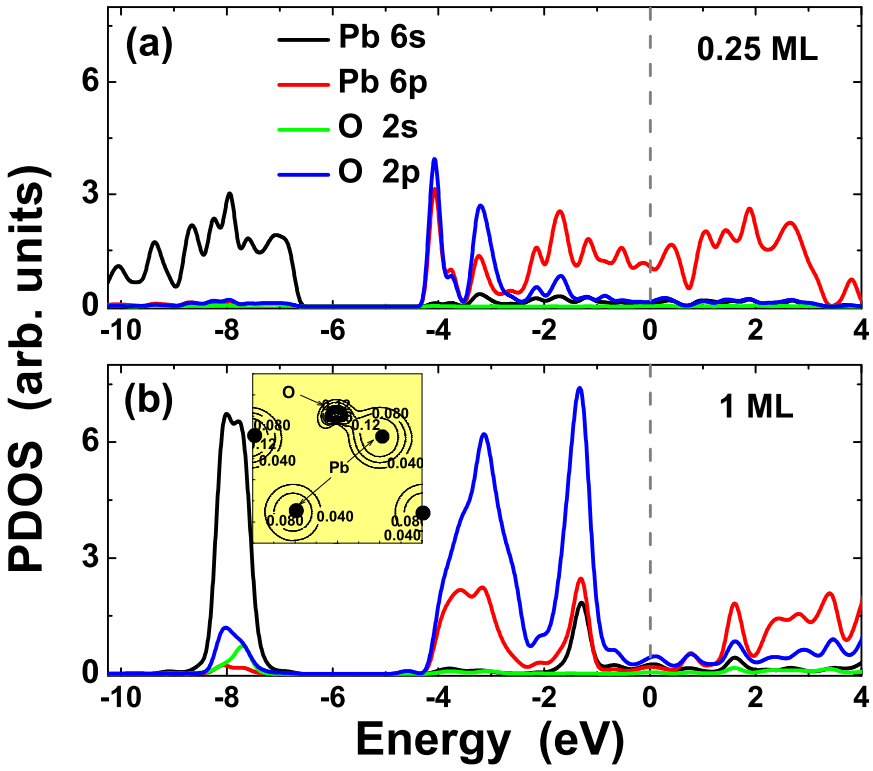

FIG. 9: (Color online) Orbital-resolved partial DOS for the surface Pb layer and the on-surface O adatom (fcc site) with the coverage (a) $\Theta = 0.25$ and (b) $\Theta = 1.0$. The inset in (b) depicts the band charge density around the energy E=-8 eV.

oxygen coverage.

Figures 9(a) and (b) show the orbital-resolved PDOS for the on-surface O_{fcc} layer and the topmost Pb layer at Θ=0.25 and Θ=1.0, respectively. At low coverage (Θ=0.25), the left-side peak [around -4.0 eV in Fig. 9(a)] of O-2p states represents the degenerate $2p_x$ and $2p_y$ states, which hybridize with the degenerate $6p_x/6p_y$ states of the outmost Pb atoms. The right-side peak [around -3.2 eV in Fig. 9(a)] of O-2p states represents the mixed $p_{x,y}$ and p_z states (with p_z orbital a little lower in energy than $p_{x,y}$ orbitals), which hybridize with Pb-$6p_{x,y}$ and -$6p_z$ states. The coupling between the Pb-6s orbital and the O-2p orbitals is negligibly small at low coverage. In addition, it shows in Fig. 9(a) that the metallic and bonding nature of surface Pb(111) layer does not change by low coverage of oxygen. This can be seen by the facts: (i) The PDOS at E_F for the topmost Pb layer is large, comparable with that for clean Pb(111) surface; (ii) The surface Pb-2s and -2p states change very little upon oxygen adsorption. In addition, the previous analysis of the atomic geometry

also showed that the change in the first-second interlayer relaxation (Δ_{12}) upon oxygen adsorption is relatively small at low coverage, indicating the metallic bonding between the first and second Pb layers preserves well. With increasing oxygen coverage, the prominent changes involving the O-Pb interaction and the surface Pb bonding occur, which can be seen from Fig. 9(b) for Θ=1.0. First, the density of the surface-layer Pb-6p states at the Fermi level is significantly suppressed. A more clear illustration can be found in Fig. 10. Second, the energy distribution of the surface-layer Pb-6s state becomes very narrow compared to its original broad-dispersion feature in the clean surface, which indicates that unlike the low-coverage case, the surface Pb s state at high coverage becomes very isolated and dense. The band charge density around the energy E=$-$8 eV is plotted in the inset in Fig. 9(b), which shows that at this energy interval, the surface Pb atoms have more and dense charge compared to the second-layer Pb atoms. Third, the energy distance between the two O-2p (or their hybridized Pb-6p) peaks increases from 0.8 eV at Θ=0.25 to 2.0 eV at Θ=1.0. Also, these two peaks become more broadened by the increase of Θ. In addition, one can see from Fig. 9(b) that at high oxygen coverage, there appears an increasing hybridization between the O-2p and the top-layer Pb-6s states around E=$-$8.0 eV. In a similar way, a hybridization between these two kinds of states at high energies around E=$-$1.3 eV also becomes obvious. For further illustration, we plot in Fig. 10 the total DOS (a sum over O_{fcc} and topmost Pb layers) for different coverages calculated by the p(2×2) surface model. One can see that the density at the Fermi energy monotonically decreases with increasing the coverage, and the metallic p bands of the topmost Pb gradually evolve into the insulating bands due to its ionic coupling with the O-2p orbitals. Also the original broad distribution of the surface Pb-2s state is increasingly narrowed with coverage. Therefore, Fig. 10 clearly the tendency to the insulating surface by the increase of the coverage.

V. THE PURE SUBSURFACE ADSORPTION

As we did in Sec. IV, we continue to study the (incorporated) subsurface adsorption of atomic oxygen without the presence of on-surface oxygen, namely, pure subsurface. For oxygen occupation in the subsurface region there are three different high-symmetry sites. The octahedral site (henceforth octa) lies just underneath the fcc on-surface site, and one tetrahedral site (tetra-I) lies below the hcp on-surface site. A second tetrahedral site (tetra-

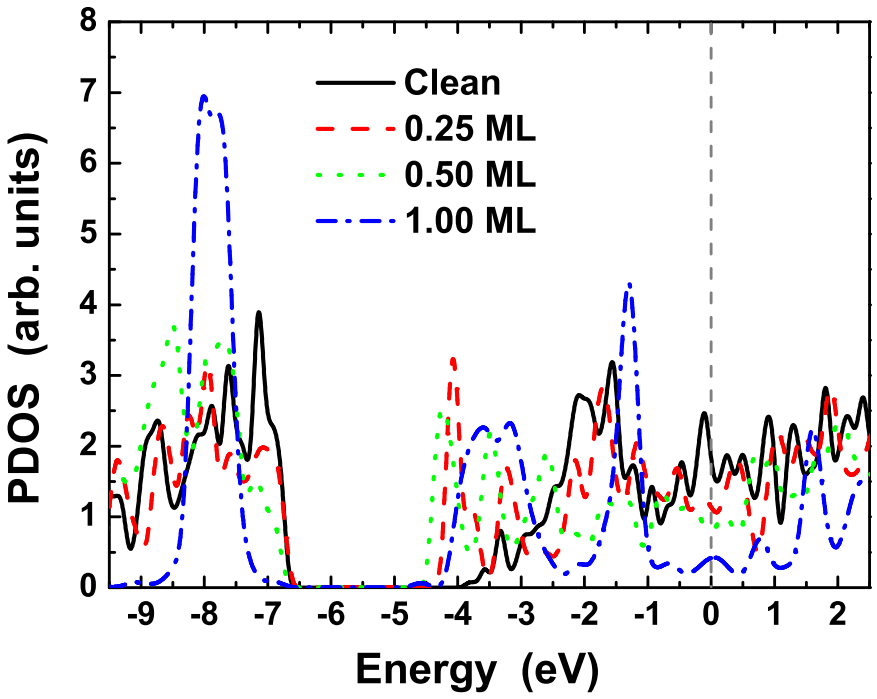

FIG. 10: (Color online) Total DOS of the on-surafec O adatoms (fcc site) and the surface-layer Pb atoms for different values of the coverage Θ.

II) is located directly below a first layer metal atom. The coordinates of these subsurface sites have been schematically shown in Fig. 1. We performed calculations for oxygen in these different sites for a wide range of coverages, i.e., from 0.11 ML to 1.0 ML. Note that we focus on adsorption immediately below the first Pb layer as we find that oxygen adsorption deep in the bulk is less favorable in every case. The cases of simultaneous subsurface and on-surface oxygen adsorption will be studied in a forthcoming paper. In the following, the subsurface energetics, the atomic structure, and the electronic properties are discussed in detail.

The calculated binding energies E_b for $O_{\text{tetra-I}}$, $O_{\text{tetra-II}}$, and O_{octa}, with respect to atomic oxygen, are plotted in Fig. 11 and summarized in Table II. It can be seen from Table II that the most preferred adsorption site is tetra-II site for the whole coverage range and among all the on-surface and subsurface adsorption sites considered. This is different from the other systems such as O/Ag(111), O/Cu(111), and O/Mg(0001). For $O_{\text{tetra-II}}$ (open circles in Fig. 11) or $O_{\text{tetra-I}}$ (open squares), the binding energy increases slightly but steadily with O coverage, which is similar to the case of on-surface adsorption. For O_{octa} adsorption (open

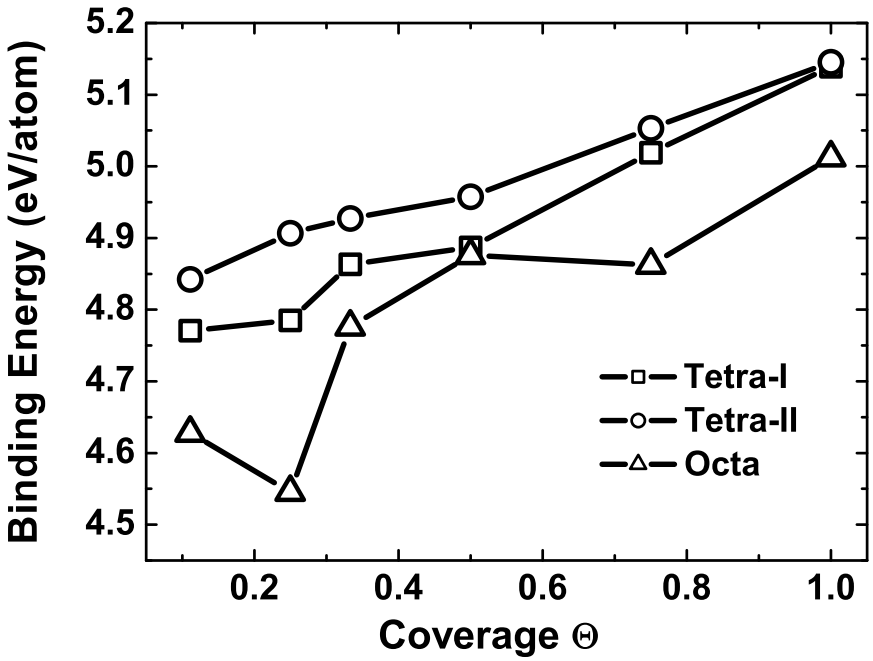

FIG. 11: Binding energies E_b for oxygen in the subsurface tetra-I, tetra-II and octa adsorption sites, as functions of the O coverage.

triangles), it reveals in Fig. 11 that the binding energy decreases when the coverage Θ varies from 0.11 to 0.25, indicating a repulsive interaction between the O_{octa} atoms; however, it increases again from Θ=0.33 to 1.0, so that the effective interaction between the O_{octa} atoms in this coverage range is attractive. Despite these different dependence on coverage, we note that the overall variation in the magnitude of the binding energy as a function of the coverage is rather small for the three subsurface sites, namely, 0.33 eV, 0.51 eV, and 0.50 eV for $O_{tetra\text{-}II}$, $O_{tetra\text{-}I}$, and O_{octa} atoms, respectively. Compared to the on-surface adsorption, the subsurface adsorption is notably more favorable in the whole range of coverages considered. In fact, the binding energy difference ΔE_b between the most energetically stable on-surface O_{fcc} and subsurface $O_{tetra\text{-}II}$ atoms increases from about 0.1 eV to 0.2 eV with increasing the coverage Θ from 0.11 to 1.0. The result that the subsurface adsorption is more stable than the on-surface adsorption has also been found in O/Mg(0001) system [52], but with the different tendency with respect to the variation of the O coverage. In the O/Mg(0001) system it was found that the value of ΔE_b decreases from about 0.4 eV to less than 0.1 eV with the increasing coverage Θ from 0.0625 to 1.0 [52].

Table IV presents the results of the O-Pb bond length R_1 and the interlayer relaxations

TABLE IV: The calculated interlayer relaxation Δ_{ij} (%) and O-Pb bond length R_1 (in Å) for different oxygen coverages of subsurface adsorption.

Coverage	R_1 (Å)			Δ_{12} (%)			Δ_{23} (%)		
Θ	tetra-I	tetra-II	octa	tetra-I	tetra-II	octa	tetra-I	tetra-II	octa
0.11	2.342	2.255	2.452	-3.238	-2.058	-3.065	2.875	1.516	1.703
0.25	2.288	2.268	2.379	0.129	0.757	0.037	3.773	2.577	0.436
0.33	2.346	2.265	2.497	-1.405	2.205	0.373	6.139	2.607	1.840
0.50	2.304	2.265	2.380	12.22	6.547	13.77	3.190	3.301	2.557
0.75	2.312	2.265	2.270	15.16	13.92	13.55	6.022	4.809	-1.861
1.00	2.351	2.254	2.327	25.18	21.80	22.25	1.407	5.420	-3.988

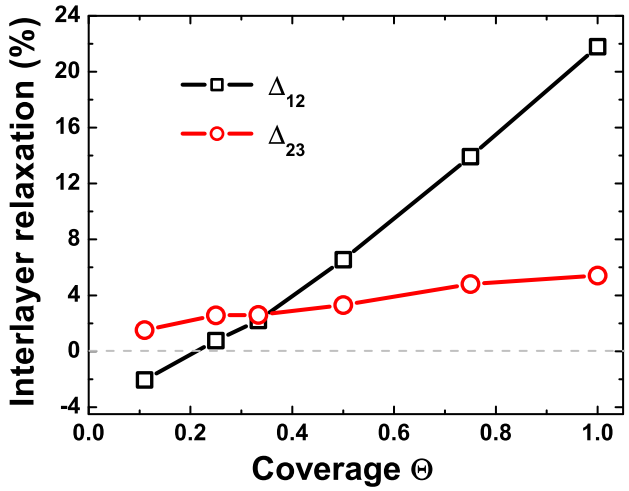

FIG. 12: Interlayer relaxations as functions of coverage for oxygen in subsurface tetra-II site.

(Δ_{12} and Δ_{23}) in a wide range of coverages for $O_{\text{tetra-I}}$, $O_{\text{tetra-II}}$, and O_{octa} atoms. For more clear illustration, the first (Δ_{12}) and second (Δ_{23}) interlayer relaxations with O in the most stable tetra-II subsurface site are also plotted in Fig. 12 as functions of Θ. The O-Pb bond length for subsurface adsorption with different coverages has been plotted in Fig. 5 together with the case of on-surface adsorption. One can see from Fig. 12 that the first interlayer relaxation Δ_{12} increases from -5% to about 22% (in a linear form) as a function of oxygen coverage, while the second interlayer relaxation Δ_{23} is much insensitive to the variation of the coverage compared to Δ_{12}. From the variation of the O-Pb bond length R_1 as a function

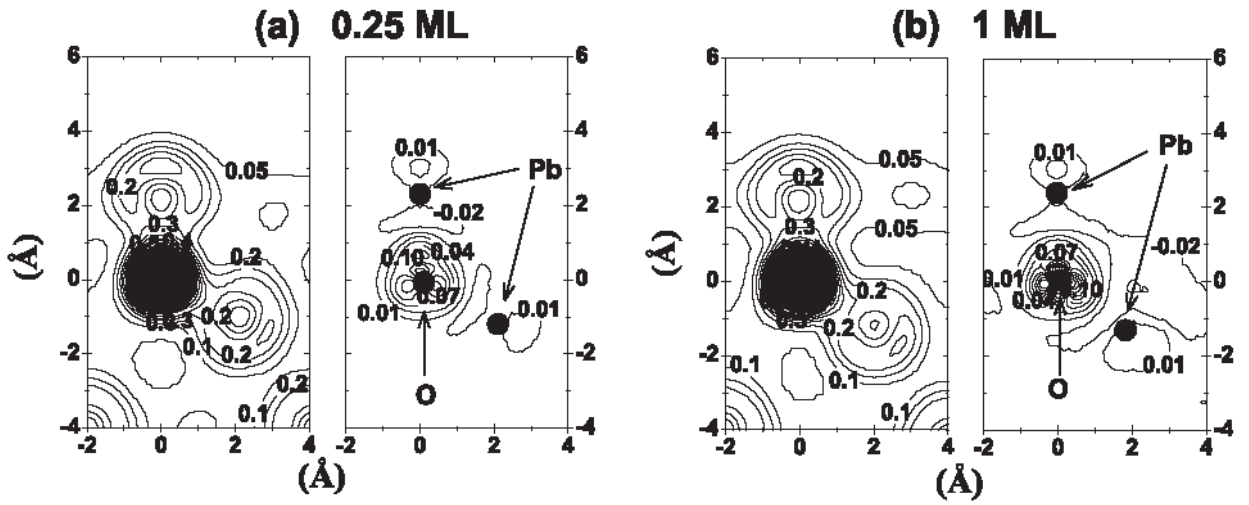

FIG. 13: Contour plots of the total charge density (left panel) and the charge density difference (right panel) for the subsurface $O_{\text{tetra-II}}$/Pb(111) slabs with the coverage (a) $\Theta = 0.25$ and (b) $\Theta = 1.0$. The contour plane is parallel with the $[1\bar{2}1]$ direction and is perpendicular to the Pb(111) surface.

of Θ (Fig. 5), one can see that the value of R_1 for $O_{\text{tetra-II}}$ atoms keeps the most shortest and stable (against Θ) compared to the other various kinds of on-surface and subsurface adsorption sites. Whereas, for the octa and tetra-I adsorption sites, it shows in Fig. 5 that the O-Pb bond length oscillates in a large amplitude with increasing Θ.

We turn now to study the electronic property of the subsurface O/Pb(111) system by first considering the work function Φ at different coverages and its change $\Delta\Phi$ with respect to the clean Pb(111) surface, both of which were illustrated in Fig. 7 and summarized in Table II. From the results shown in Fig. 7(a), it can be seen that the work function slightly but steadily decreases with the coverage for three subsurface adsorption sites. The overall variation in the magnitude of the $\Delta\Phi$ is rather small, namely, -0.8 eV, -0.66 eV, and -0.73 eV for $O_{\text{tetra-II}}$, $O_{\text{tetra-I}}$, and O_{octa}, respectively. These results of $\Delta\Phi$ versus Θ can be comparable with those in O/Al(111) system [48], in which relatively small work-function change was observed despite the strong electron transfer between adsorbate and Al atoms, and was associated with the small adsorption distance for the O species [69]. Also from Figs. 7(a)-(b) it can be seen that the amplitude of $\Delta\Phi$ for the tetra-II adsorption is most prominent among the three subsurface sties.

To gain more insight into the nature of the O subsurface adsorption, we now analyze our results by means of the charge density difference $\Delta n(\mathbf{r})$. Figures 13(a)-(b) (right panel in each figure) present the contour plots of $\Delta n(\mathbf{r})$ for Θ=0.25 and Θ=1.0, respectively, for the tetra-II subsurface adsorption. The total charge densities are also shown in the left panels. It reveals that the charge redistribution mainly involves the subsurface O and the neighboring outmost two Pb layers. The electrons flows upon adsorption from the first- and second-layer Pb atoms to the O-2p orbitals. It is apparent that the adsorbed O-2p orbitals are not the same as those of the free O atom but they are polarized along the three Pb-O axis. This polarization is reasonable because the Pb atoms are positively charged. Also one can see from Fig. 13 that the bonding character of the inner Pb layers (from the third layer for the whole coverages considered) is essentially identical to the bulk case, while the first- and second-layer Pb atoms show remarkable changes in the charge density, reflecting the strong influence of the neighboring subsurface O atom. As with the on-surface adsorption, since there is no electron density accumulation in the O-Pb bondng regions, we obtain an ionic-like bonding picture for the subsurface O atom, with charge transfer and polarization. The subsurface accumulation and the on-surface depletion in the charge density would result in the formation of a dipole moment (anti-paralleling with the usual surface dipole layer) which tends to reduce the work function as compared to that for the clean Pb(111) surface, as shown in Fig. 7.

Figures 14(a)-(b) shows the PDOS for the subsurface $O_{\text{tetra-II}}$ layer and the first and second Pb(111) layers at coverages Θ=0.25 and Θ=1.0, respectively. Similarly to on-surface oxygen adsorption, the interaction between subsurface oxygen and lead is mainly via hybridization of the O-2p and Pb-6sp states. During this hybridization, however, the PDOS energy distribution of two Pb layers and of the 6s and 6p orbitals of the same Pb layer are prominently different. In fact, it can be seen from Fig. 14(a) that at low coverage, the O-2p states mainly hybridize with the Pb-6p states, while the interaction between the O-2p states and the Pb-6s states is negligibly small. The O-2p states couple to 6p states of the second Pb layer more strongly than those of the first Pb layer, since the two peaks around -4 eV (below the Fermi energy) in Fig. 14(a) mainly consist of 2p states of $O_{\text{tetra-II}}$ atoms and 6p states of the second Pb layer, while the contribution from the first-layer Pb atoms is small. The reason is simply due to the fact that at low coverage, every $O_{\text{tetra-II}}$ atom is bonded to its four neighboring Pb atoms, three of which come from the second Pb layer, while only

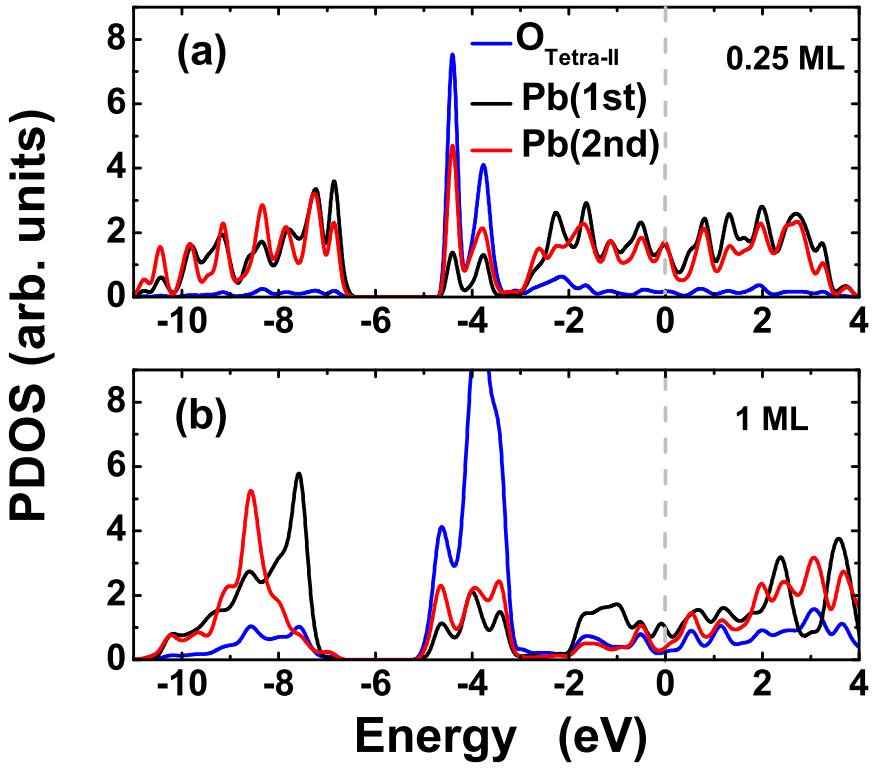

FIG. 14: (Color online) Layer-projected DOS for the $O_{tetra-II}$ subsurface layer and the outmost two Pb(111) layers.

one comes from the first Pb layer. At as high coverage as Θ= 1.0 [Fig. 14(b)], there are the following new features: (i) The PDOS shifts downwards in energy and a large spectra weight near the Fermi energy (from below) becomes very small, both of which obviously will lead to the increase in the adsorption energy; (ii) The coupling between the O-2p and Pb-2s states comes to play an important role in the O-Pb bond. Due to the difference in the coordinates of the neighboring Pb atoms, this coupling is asymmetric for the first- and second-layer Pb atoms, thus giving rise to a weight splitting in the 6s PDOS of the two Pb layers as shown in Fig. 14(b); (iii) With increase of $O_{tetra-II}$ coverage, the coupling between the O-2p states and first-layer Pb-2p states is enhanced, which is revealed by the peaks around -4.0 eV (below the Fermi energy) in Fig. 14(b); (iv) Compared to the high-coverage on-surface adsorption [Fig. 9(b)], the narrowing effect of the Pb-2s DOS by the coupling with O-2p states is not prominent so much.

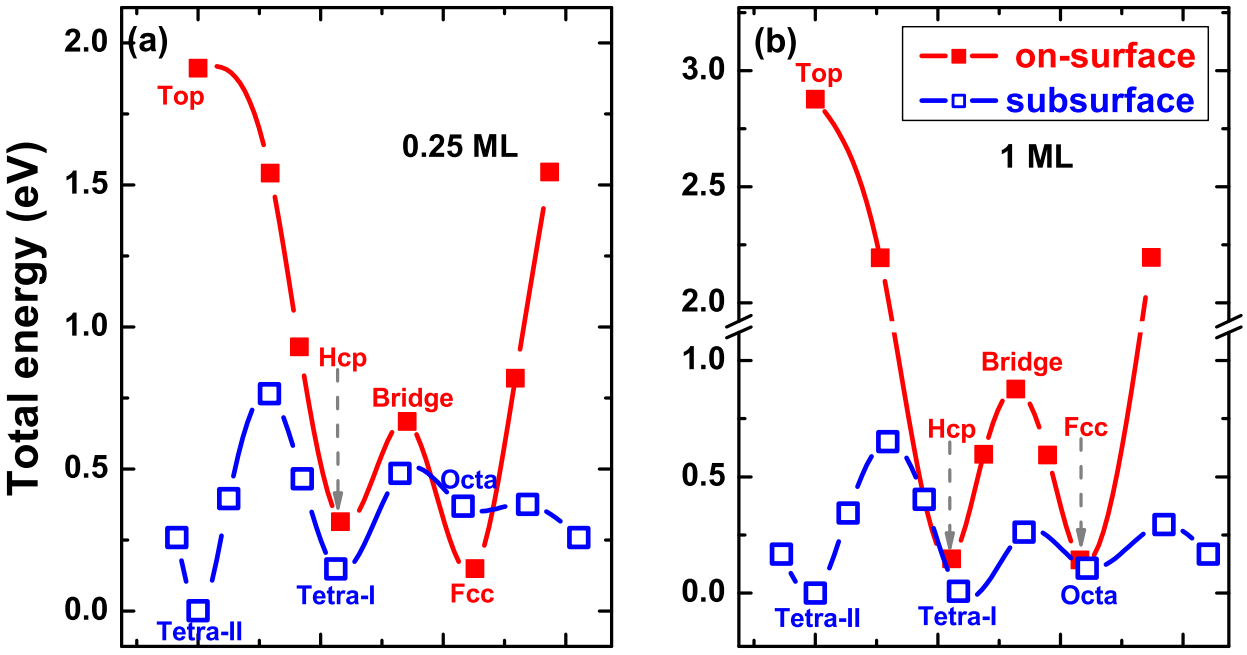

FIG. 15: (Color online) Total energy for an oxygen atom carrying out the on-surface (filled squares) or the subsurface (open squares) diffusion on Pb(111) face at the O coverage of (a) $\Theta = 0.25$ and (b) $\Theta = 1.0$. Here the total energy is given in reference to the most stable subsurface tetra-II occupation.

VI. THE ENERGY BARRIER FOR ATOMIC OXYGEN DIFFUSION

The diffusion of the atomic O after the on-surface dissociation of the O_2 molecule is an elementary process during the whole surface oxidation process, which is still in debate for many systems regarding the existence of "hot" atoms with transient mobility upon O_2 dissociation [70–72]. Also, the oxygen diffusion plays a key role in understanding many important catalytic reactions, such as oxidation of CO and hydrocarbons in the catalytic treatment of the automotive exhaust gases. In this section, by using the DFT total energy calculation, we report our numerical results of the energy barriers for atomic O diffusion and penetration in the O/Pb(111) system.

Using the nudged elastic band (NEB) method [73–75], which is capable of finding saddle points and minimum energy paths on complicated potential surfaces, we have calculated the on-surface and subsurface diffusion-path energetics of atomic oxygen. The results are shown in Fig. 15(a) for low (Θ=0.25) coverage and in Fig. 15(b) for high (Θ=1.0) coverage.

Note that in each figure [Fig. 15(a) or (b)] the number of atoms keeps invariant in the on-surface and subsurface calculations. Thus it also reveals in Fig. 15 the relative stability of O adsorption among various on-surface and subsurface sites and the corresponding oxygen binding energy differences. For the on-surface adsorption, our calculated diffusion barrier from fcc to hcp site is 0.52 eV at Θ=0.25 and 0.74 eV at Θ=1.0. The hcp site is less stable than the fcc site within the coverages $0 < \Theta \leq 1$, although the binding energy difference between O_{fcc} and O_{hcp} decreases rapidly when increasing Θ (see Fig. 3). Thus the on-surface diffusion barrier from hcp to fcc site presents an activation barrier with the value of 0.35 eV at Θ=0.25 and of 0.73 eV at Θ=1.0. For the subsurface adsorption, Fig. 15 shows that all of the three sites we considered, i.e., the tetra-I, the tetra-II and the octa sites present the local energy minimum along the oxygen subsurface diffusion path. The subsurface diffusion barrier from tetra-II to tetra-I is 0.76 eV at Θ=0.25 and 0.64 eV at Θ=1.0. For the diffusion from the tetra-I site to the octa site, the calculated energy barrier is 0.28 eV at Θ=0.25 and 0.25 eV at Θ=1.0. For the diffusion from the tetra-II to octa site, the calculated barrier is 0.37 eV at Θ=0.25 and 0.29 eV at Θ=1.0. The octa site is less stable than the tetra-I site, while the tetra-I site is less stable than the tetra-II site. Thus the subsurface diffusion barrier from tetra-I to tetra-II site presents an activation barrier with the value of 0.62 eV at Θ=0.25 and of 0.64 eV at Θ=1.0. In the same way, the activation barrier for octa$\rightarrow$tetra-I diffusion is 0.11 eV at Θ=0.25 and 0.16 eV at Θ=1.0, while the activation barrier for octa$\rightarrow$tetra-II diffusion is 0.01 eV at Θ=0.25 and 0.18 eV at Θ=1.0.

To investigate subsurface oxygen in more detail with regard to the energetics of its formation, we now study the penetration process of oxygen atom. Note that although the subsurface tetra-II site is most stable, the direct oxygen penetration into this site from the on-surface adsorption without by-passing the other subsurface sites is very unfavorable, since this site is located below a surface Pb atom. Therefore, here we only consider the penetration of O atom through the outmost Pb layer from the on-surface fcc (hcp) to the neighboring subsurface octa (tetra-I) site at the coverage Θ=0.25. For this purpose, we fully relaxed the first three Pb layers, and restrain the oxygen atom when approaching to the first Pb layer step by step to search for the transition state with high energy. The calculated penetration paths and the energy barriers from the on-surface fcc to subsurface octa site and from the on-surface hcp to subsurface tetra-I site are shown in Fig. 16, in which the s coordinate indicates the penetration distance of the O atom with respect to the initial

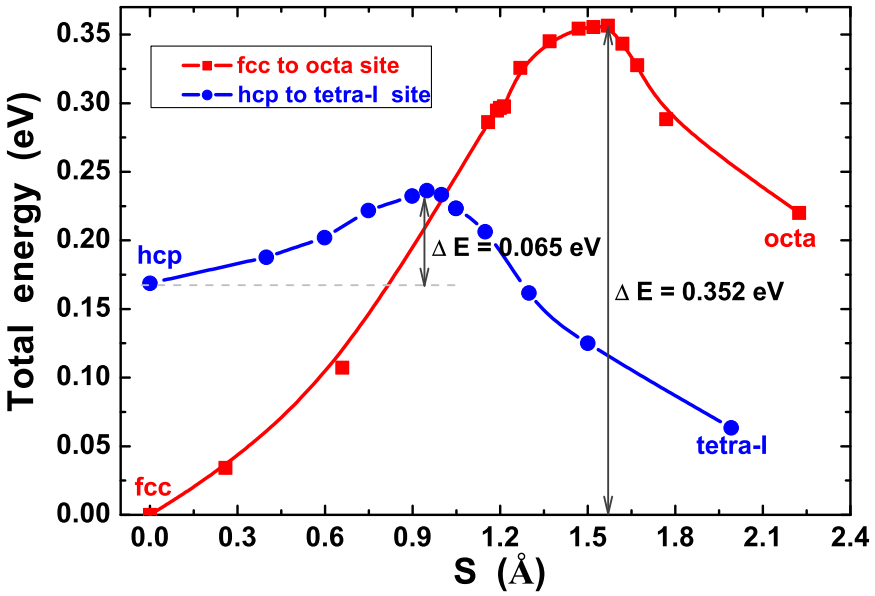

FIG. 16: (Color online) Total energy for an oxygen atom carrying out the penetration from the on-surface fcc to the subsurface octa site (filled squares) or from the on-surface hcp to the subsurface tetra-I site (filled circles) of Pb(111) lattice. Here the O coverage is set $\Theta = 0.25$ and the total energy is given in reference to the on-surface fcc occupation. s coordinate indicates the penetration distance of the O atom with respect to the initial on-surface fcc or hcp adsorption site.

on-surface fcc or hcp adsorption site. The calculated penetration barrier from on-surface fcc to subsurface octa site is 0.352 eV. The transition state, i.e., the atomic geometry of the energy maximum in the penetration path, corresponds to the oxygen atom 0.1 Åabove the surface Pb layer. For penetration from the on-surface hcp to the subsurface tetra-I site, the calculated activation barrier is as small as 0.065 eV, which implies the most favorable path for the oxygen penetration. The transition state corresponds to the oxygen atom 0.4 Å below the surface Pb layer. Comparing to the energy barriers for the O on-surface diffusion, one can see that the oxygen atoms can easily intrude into the subsurface and bond with the second-layer Pb atoms rather than searching for a more stable on-surface site (fcc site) to settle down. Even though an oxygen atom settles down at the stable on-surface fcc site, it also can penetrate into the subsurface stimulated by a slight perturbation.

VII. CONCLUSION

In summary, we have systematically investigated the adsorption of atomic oxygen on the Pb(111) surface and subsurface, as well as the energy barriers for atomic O diffusion and penetration in these systems through first-principles DFT-GGA calculations. We considered a wide range of coverage using different surface models [i.e., p(3×3), p(2×2), p($\sqrt{3} \times \sqrt{3}$), and p(1×1) surface unit cells] for adsorption in the on-surface fcc and hcp sites as well as the subsurface tetra-I, tetra-II, and octa sites. For the on-surface adsorption, the fcc site is more stable than the hcp site for the whole coverage range considered. The oxygen binding energy difference between these two sites decreases with increasing coverage. In particular, at the coverage of 1 ML, the binding energy of O_{hcp} is almost identical from below to that of O_{fcc}, implying a critical coverage for the stability conversion between the on-surface fcc and hcp sites. The atomic geometry, the work-function change, the charge density distribution, and the electronic structure upon the O on-surface adsorption have also been studied, which consistently show the fundamental influence by the ionic bonding between the O atom and the first-layer Pb atoms with charge transfer from the latter to the former. Remarkably, this influence in the energetics and atomic structure is monotonically enhanced with increasing the O coverage, which is highly interesting. For instance, the increase of the O binding energy for the fcc or the hcp site with increasing the coverage implies the effective attraction between the O adsorbates, which will make it favorable for the formation of the oxygen island or cluster. Furthermore, we have found that with increasing coverage, the electronic PDOS at the Fermi energy rapidly decreases, which will further stabilize the system in accordance with the increase in binding energy.

For the purely subsurface O adsorption, the tetra-II site is more stable than the tetra-I and octa sites for the whole coverage range considered. A similar correlation between the binding energy and the coverage has been found for $O_{tetra\text{-}I}$ and $O_{tetra\text{-}II}$, which also implies the effective attraction between the adsorbed O atoms and the tendency to form the oxygen island or cluster at subsurface sites. The other atomic and electronic structural properties of the subsurface adsorption have also been investigated. The observed increase of the first-second Pb interlayer expansion, the decrease of the work-function change $\Delta\Phi$, and the decrease of the PDOS at the Fermi energy as functions of the O coverage, consistently show the stabilization of the ionic O-Pb bond with the charge transfer from the first- and

second-layer Pb atoms to the subsurface O atom.

Given the observation that the oxygen atom is more stable for the subsurface than for the on-surface adsorption, we have calculated the on-surface and subsurface diffusion-path energetics of O. The activation barrier for the on-surface or the subsurface O diffusion becomes high when increasing the coverage, which indicates the competition between the attractive interaction from the adsorbate and the substrate and the repulsive force among the adsorbates. In particular, we have shown that the activation barrier for the penetration from the on-surface hcp to the subsurface tetra-I site is as low as 0.065 eV, which indicates that the oxygen atoms can directly incorporate into the lead (below the topmost Pb layer) right after on-surface O_2 dissociation at low coverage rather than nearly completion of a dense O adlayer.

Acknowledgments

This work was supported by the NSFC under grants Nos. 10604010 and 10544004.

---

[1] K. Thürmer, E. Williams, and J. Reutt-Robey, Science **297**, 2033 (2002).

[2] P. Jiang, X. Ma, L.L. Wang, Y.S. Fu, S.H. Ji, Y. Qi, J. Jia, and Q.-K. Xue, to be published.

[3] X. Ma, P. Jiang, Y. Qi, J. Jia, Y. Yang, W. Duan, W.-X. Li, X. Bao, S.B. Zhang, and Q.-K. Xue, Proc. Natl. Acad. Sci. U.S.A. **104**, 9204 (2007).

[4] P. Jiang, X. Ma, Y. Yang, Y.X. Ning, L.L. Wang, Y.S. Fu, S.H. Ji, Y. Qi, W. Duan, S.B. Zhang, J. Jia, and Q.-K. Xue, to be published.

[5] M. Alatalo, S. Jaatinen, P. Salo and K. Laasonen, Phys. Rev. B **70**, 245417 (2004), and references therein.

[6] S. Jaatinen, J. Blomqvist, P. Salo, A. Puisto, M. Alatalo, M. Hirsimäki, M. Ahonen, and M. Valden, Rev. B **75**, 075402 (2007).

[7] J.C. Yang, B. Kolasa, J.M. Gibson, and M. Yeadon, Appl. Phys. Lett. **73**, 2841 (1998).

[8] Y. Xu and M. Mavrikakis, Surf. Sci. **494**, 131 (2001).

[9] A. Soon, M. Todorova, B. Delley, and C. Stamplf, Rev. B **73**, 165424 (2006).

[10] G. Ertl, Surf. Sci. **6**, 208 (1967).

[11] J. Haase and H. J. Kuhr, Surf. Sci. **203**, L695 (1988).

[12] F. Jensen, F. Besenbacher, E. Lægsgaard, and I. Stensgaard, Surf. Sci. **259**, L774 (1991).

[13] S.M. Johnston, A. Mulligan, V. Dhanak, and M. Kadodwala, Surf. Sci. **519**,57 (2002).

[14] M. Rocca, L. Savio, L. Vattuone, U. Burghaus, V. Palomba, N. Novelli , F. Buatier de Mongeot, and U. Valbusa, Phys. Rev. B **61**, 213 (2000).

[15] L. Savio, L. Vattuone, M. Rocca, F. Buatier de Mongeot, G. Comelli, A. Baraldi, S. Lizzit, and G. Paolucci, Surf. Sci. **506**, 213 (2002).

[16] M.A. Barteau and R.J. Madix, J. Electron Spectrosc. Relat. Phenom. **31**, 101 (1983).

[17] C.T. Campbell and M.T. Paffett, Surf. Sci. **143**, 517 (1984).

[18] V.I. Bukhtiyarov, V.V. Kaichev, and I.P. Prosvirin, J. Chem. Phys. **111**, 2169 (1999).

[19] C. T. Cambell, Surf. Sci. **173**, L641 (1986), and references therein.

[20] W.-X. Li, C. Stampfl, and M. Scheffler, Phys. Rev. B **65**, 075407 (2002).

[21] W.-X. Li, C. Stampfl, and M. Scheffler, Phys. Rev. B **67**, 045408 (2003).

[22] M.-L. Bocquet, A. Michaelides, P. Sautet, and D.A. King, Phys. Rev. B **68**, 075413 (2003).

[23] G. Rovida, F. Pratesi, M. Maglietta, and E. Ferroni, Surf. Sci. **43**, 230 (1974).

[24] C.T. Campbell, Surf. Sci. **157**, 43 (1985).

[25] C.I. Carlisle, D.A. King, M.L. Bocquet, J.Cerdá and P. Sautet, Phys. Rev. Lett. **84**, 3899 (2000).

[26] M. V. Ganduglia-Pirovano and M. Scheffler, Phys. Rev. B **59**, 15533 (1999).

[27] M.V. Ganduglia-Pirovano, K. Reuter, and M. Scheffler, Phys. Rev. B **65**, 245426 (2002).

[28] G. Comelli, V.R. Dhanak, M. Kiskinova, K.C. Prince, and R. Rosei, Surf. Sci. Rep. **32**, 165 (1998), and references there in.

[29] M.V. Ganduglia-Pirovano and M. Scheffler, Phys. Rev. B **59**, 15533 (1999).

[30] J. Wider, T. Greber, E. etli, T.J. Kreutz, P. Schwaller, and J. Osterwalder, Surf. Sci. **417**, 301 (1998); **432**, 170 (1999).

[31] E. Lundgren, G. Kresse, C. Klein, M. Borg, J.N. Andersen, M. De Santis, Y. Gauthier, C. Konvicka, M. Schmid, and P. Varga, Phys. Rev. Lett **88**, 246103 (2002), and references therein.

[32] G. Zheng and E. I. Altman, Surf. Sci. **462**, 151 (2000).

[33] A. P. Seitsonen, Y. D. Kim, S. Schwegmann, and H. Over, Surf. Sci. **468**, 176 (2000).

[34] M. Todorova, K. Reuter, and M. Scheffler, J. Phys. Chem. B **108**, 14477 (2004).

[35] M. Todorova, K. Reuter, and M. Scheffler, Phys. Rev. B **71**, 195403 (2005).

[36] W.-X. Li, L. Österlund, E.K.Vestergaard, R.T.Vang, J. Matthiesen, T.M. Pedersen, E. Laegsgaard, B. Hammer, and F. Besenbacher, Phys. Rev. Lett. **93**, 146104 (2004).

[37] J. L. Gland, Surf. Sci. **93**, 487 (1980).

[38] A. Eichler and J. Hafner, Phys. Rev. Lett. **79**, 4481 (1997).

[39] A. Bogicevic, J. Strömquist, and B.I. Lundqvist, Phys. Rev. B **57**, 4289 (1998).

[40] H. Tang, A.V. der Ven, and B.L. Trout, Phys. Rev. B **70**, 045420 (2004).

[41] K. Reuter, M.-V. Ganduglia-Pirovano, C. Stampfl, and M. Scheffler, Phys. Rev. B **65**, 165403 (2002).

[42] C. Stampfl, S. Schwegmann, H. Over, M. Scheffler, and G.Ertl, Phys. Rev. Lett. **77**, 3371 (1996).

[43] K. Honkala, and K. Laasonen, Phys. Rev. Lett. **84**, 705 (2000).

[44] T. Sasaki, and T. Ohno, Phys. Rev. B **60**, 7824 (1999).

[45] L.C. Ciacchi, and M.C. Payne, Phys. Rev. Lett. **92**, 176104 (2004).

[46] J. Behler, B. Delley, S. Lorenz, K. Reuter, and M. Scheffler, Phys. Rev. Lett. **94**, 036104 (2005).

[47] J. Jacobsen, B. Hammer, K.W. Jacobsen, and J.K. Nørskov, Phys. Rev. B **52**, 14954 (1995).

[48] A. Kiejna and B.I. Lundqvist, Phys. Rev. B **63**, 085405 (2001), and references therein.

[49] A. Kiejna, Phys. Rev. B **68**, 235405 (2003).

[50] A. Hellman, Phys. Rev. B **72**, 201403 (2005).

[51] E. Schröder, R. Fasel, and A. Kiejna, Phys. Rev. B **69**, 193405 (2004).

[52] E. Schröder, R. Fasel, and A. Kiejna, Phys. Rev. B **69**, 115431 (2004), and references therein.

[53] G. Kresse and J. Hafner, Phys. Rev. B **47**, 558 (1993); G. Kresse and J. Furthmüller, Comput. Mater. Sci. **6**, 15 (1996); G. Kresse and J. Furthmüller, Phys. Rev. B **54**, 11169 (1996).

[54] G. Kresse and D. Joubert, Phys. Rev. B **59**, 1758 (1999).

[55] M. Bockstedte, A. Kley, J. Neugebauer, and M. Scheffler, Comput. Phys. Commun. **107**, 187 (1997).

[56] *Princinciples of Surface Physics*, edited by F. Bechstedt (Springer, Verlag Berlin Heidelberg, 2003).

[57] J. Neugebauer and M. Scheffler, Phys. Rev. B **46**, 16067 (1992).

[58] J.P. Perdew et al., Phys. Rev. B 46, 6671 (1992).

[59] M. Weinert and J.W. Davenport, Phys. Rev. B **45**, 13709 (1992).

[60] H.J. Monkhorst and J.D. Pack, Phys. Rev. B **13**, 5188 (1976).

[61] C. Kittel, *Introduction to Solid State Physics,* 5th ed. (Wiley, New York, 1976).

[62] G.W. Watson, S.C. Parker, G. Kresse, Phys. Rev. B **59**, 8481 (1999).

[63] D.J. Payne, R.G. Egdell, G. Paolicelli, F. Offi, G. Panaccione, P. Lacovig, G. Monaco, G. Vanko, A. Walsh, G.W. Watson, J. Guo, G. Beamson, P.-A. Glans, T. Learmonth, and K. E. Smith, Phys. Rev. B **75**, 153102 (2007).

[64] To test the Pb 5d electron effect, the O/Pb(111) system has been calculated by treating Pb 5d electrons as valence electrons at a 0.25 ML coverage. The Pb 5d states are found to be localized in the deep energy levels ranging from about -17 eV to -16 eV, with a weak hybridization with O 2s states. The calculated physical properties including the binding energy, work functuion, and interlayer relaxations show that the consideration of Pb 5d electrons (as valence electrons) does not change the preferred adsorption site for on-surface and subsurface adsorption. The binding energy has a very little increase of about 0.1 eV in quantity due to the consideration of Pb 5d electrons. But the work function, the Pb-O bonding length, and the interlayer relaxations are found to be quite similar to the results without considering the Pb 5d electrons.

[65] Y. Jia, B. Wu, H.H. Weitering, and Z.Y. Zhang, Phys. Rev. B **74**, 035433 (2005).

[66] A. Mans, J.H. Dil, A.R.H.F. Ettema, and H.H. Weitering, Phys. Rev. B **72**, 155442 (2005).

[67] H. Krakauer, M. Posternak, A.J. Freeman, and D.D. Koelling, Phys. Rev. B **23**, 3859 (1981).

[68] K.P. Huber and G. Herzberg, *Molecular Spectra and Molecular Structure IV: Constants of Diatomic Molecules* (Van Nostrand Reinhold, New York, 1979).

[69] N.D. Lang, Surf. Sci. **127**, L118 (1983).

[70] J. Wintterlin, R. Schuster, and G. Ertl, Phys. Rev. Lett. **77**, 123 (1996).

[71] J. Harris and B. Kasemo, Surf. Sci. **105**, L281 (1981).

[72] H. Brune, J. Wintterlin, J. Trost, G. Ertl, J. Wiechers, and R.J. Behm, J. Chem. Phys. **99**, 2128 (1993).

[73] G. Mills and H. Jónsson, Phys. Rev. Lett. **72**, 1124 (1994).

[74] G. Mills, H. Jónsson, and G. Schenter, Surf. Sci. **324**, 305 (1995).

[75] M. Alatalo, S. Jaatinen, P. Salo and K. Laasonen, Phys. Rev. B **70**, 245417 (2004).